COUPLED HYGRO-MECHANICAL (CHM) MESO-SCALE ANALYSIS OF LONG-TERM CREEP AND SHRINKAGE OF CONCRETE CYLINDERS

GEKOPPELTE HYGROMECHANISCHE MESOANALYSE DES LANGFRISTIGEN KRIECHENS UND SCHWINDENS VON BETONZYLINDERN

Joško Ožbolt, Serena Gambarelli, Sekandar Zadran

Materials Testing Institute (MPA), University of Stuttgart, Otto-Graf-Institute

SUMMARY

In the present study the interaction between the load-induced damage of concrete and its non-elastic time deformations, drying shrinkage and basic creep of mortar, is numerically investigated through a 3D meso-scale finite element (FE) simulation. The transient numerical analysis is performed by employing two-phase meso-scale FE discretization of concrete (aggregate and mortar). The constitutive law for mortar is based on the hygro-mechanical model, which couples the Fickian moisture transport and the microplane-based mechanical model. After calibration and verification of the model a parametric study is carried out for the sustained tensile and compressive load. It is shown that the meso-scale model for concrete is able to replicate the long-term experimental tests for drying creep based only on the interaction between damage, drying shrinkage and basic creep, without the need for any additional viscos kind of mortar strains due to drying. The parametric study showed that there is a strong interaction between drying shrinkage, the load-induced damage of mortar and heterogeneity of concrete. This mainly contributes to drying creep of concrete and leads to the reduction of uniaxial compressive strength to approximately 80% of short-term strength. For tensile load the interaction is even stronger and causes the reduction of short-term tensile strength to approximately 40%. The study also indicates that there is no strong interaction between the load-induced damage and basic creep of mortar.

ZUSAMMENFASSUNG

In der vorliegenden Studie wird mit einer 3D-Finite-Elemente-Simulation (FE) im Mesomassstab die Wechselwirkung zwischen der lastinduzierten Schädigung des Betons und seinen nichtelastischen zeitlichen Verformungen numerisch untersucht, welche sich mit dem Trocknungsschwinden des Mörtels und dem Grundkriechen des Mörtels berechnen. Die instationäre numerische Analyse wird unter Verwendung einer zweiphasigen FE-Diskretisierung von Beton (Gesteinskörnungen und Mörtel) durchgeführt. Das konstitutive Gesetz für den Mörtel basiert auf dem hygro-mechanischen Modell, das den Fickschen Feuchtigkeitstransport mit dem mechanischen Microplane Model verbindet. Nach der Kalibrierung und Überprüfung des Modells wird eine parametrische Studie für langzeitige Zug- und Druckbelastungen durchgeführt. Es wird gezeigt, dass das Mesomodell für Beton in der Lage ist, die experimentellen Langzeitversuche zum Trocknungskriechen treffend darzustellen, wobei die Modellparameter nur auf der Interaktion zwischen Schädigung, Trocknungsschwinden und Basiskriechen basieren, ohne dass eine zusätzliche viskose Art von Mörteldehnungen infolge der Trocknung erforderlich ist. Die parametrische Studie zeigt, dass es eine deutliche Wechselwirkung zwischen dem Trocknungsschwinden, der lastbedingten Schädigung des Mörtels und der Heterogenität des Betons existiert. Diese trägt hauptsächlich zum Trocknungskriechen des Betons bei und führt zu einer Verringerung der einachsigen Druckfestigkeit auf etwa 80 % der Kurzzeitdruckfestigkeit. Bei Zugbelastung ist die Wechselwirkung sogar noch ausgeprägter und bewirkt eine Verringerung der Kurzzeitzugfestigkeit auf etwa 40%. Die Studie zeigt auch, dass es keine deutliche Wechselwirkung zwischen der lastinduzierten Schädigung und dem Grundkriechen des Mörtels gibt.

1. INTRODUCTION

A phenomenological understanding of time-dependent phenomena in concrete, such as creep and shrinkage, is fundamental for reliable prediction of the long-term performance of concrete structures. The time-dependent processes (creep, shrinkage, variation of thermal strains and humidity) of concrete take place at the level of hardened cement paste. In particular, the creep deformation under sustained load has two contributions, namely: basic creep, which is measured at constant temperature and humidity, and drying creep, which is an additional creep associated with the moisture content variation between C-S-H sheets. Due to the

heterogeneous structure of concrete, creep at concrete level (macro level) becomes more complex than the creep of hardened cement paste. The entity and type of the applied sustained load, e.g., compression or tension, greatly influence the long-term deformation of concrete.

Over the years, several researchers experimentally investigated the long-term creep and shrinkage of concrete [1-2]. From the results it is evident that the time-dependent deformation of concrete is mainly controlled by several parameters, which can be divided into two categories: (i) intrinsic parameters of the concrete mix (geometrical and mechanical properties of the aggregate), and (ii) extensive parameters, such as the load level, environmental conditions, degree of hydration and pore water content.

A number of numerical approaches can be found in the literature for modelling of time-dependent behavior of concrete [3-5]. Some older studies [3] are based on the simplified empirical formula describing the average shrinkage and creep over a cross section. More advanced numerical approaches introduce coupled hygro-thermo-mechanical (HTM) models to realistically capture the main effects of variable environmental conditions on creep of concrete [6-10].

It is worth mentioning that all the aforementioned models are formulated in the framework of the macroscale modelling approach, therefore they cannot explicitly account for the contribution of the material heterogeneity on the creep of concrete. With these premises, the main aim of the present study is to investigate how the non-elastic time deformation of mortar (basic creep and drying shrinkage) together with the load induced damage and heterogeneity of concrete influence the drying creep of concrete. The hygro-mechanical model, which couples the micro-plane-based mechanical model with the Fickian moisture transport formulation is employed. To filter out only the influence of the load-induced damage of mortar on the time-dependent response of concrete, it is assumed that there is no interaction between basic creep and shrinkage of mortar (cement paste), i.e. only mechanical interaction between the load-induced damage of mortar and its non-elastic deformation (basic creep and drying shrinkage) is considered. Moreover, it is assumed that basic creep is independent of humidity.

2. 3D MESO-SCALE FINITE ELEMENT MODEL

2.1 Geometry and FE discretization

In this study the geometry of the test specimen is the same as in the experimental study of Kristiawan [11] (appropriate for tension & compression) and Brooks [12] (appropriate only for compression). The analyzed specimen has the shape of bobbin (Fig. 1a), i.e. it is a cylinder with diameter of 76 mm and the height of 265 mm. The specimen ends have larger diameter (110 mm) to form truncated cones that is convenient for the longterm tests of concrete under tensile load.

The finite element discretization of the bobbin-shaped specimen at the meso-scale is shown in Fig. 1b. To generate two-phase (mortar and aggregate) meso-scale structure of concrete, the coarse aggregate, assumed spherical, is randomly distributed inside the concrete specimen by employing a generation procedure developed in Matlab R2013b. In the procedure two distance criteria are used: the first one avoids contact between the external boundaries of the specimen and the generated spheres and the second one avoids the intersection between the particles. The size distribution of the coarse aggregate is determined by using the Fuller curve (Eq. 1):

$$p(d) = 100\left(\frac{d}{d_{max}}\right)^{q} \tag{1}$$

where *p(d)* is the corresponding passing amount (%), *d* is the diameter of each granulometric class, *d_max* is the maximum aggregate diameter and *q* is the exponent of the chosen granulometric curve. A volume fraction of 28% of the coarse aggregate (6 mm ≤ d ≤ 12 mm) is obtained in the model.

The geometry of the created meso-models was imported into the 3D FE code MASA used for the simulations and meshed with approximately 550000 solid four-node constant strain finite elements.

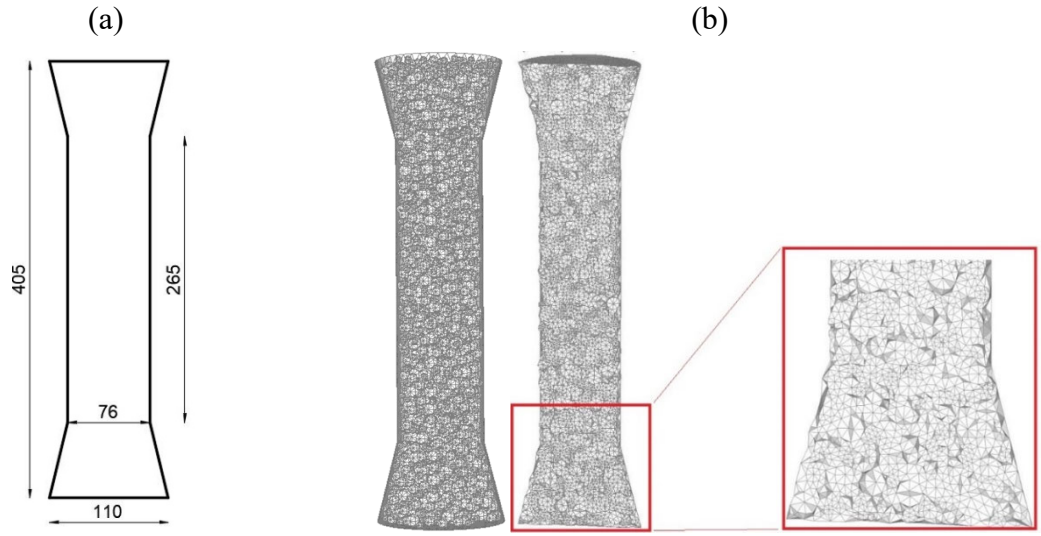

Fig 1: (a) Geometry of the specimen and (b) finite element discretization at meso scale

2.2 Constitutive law

In the two-phase meso-scale model the constitutive law for mortar is based on the strain rate insensitive microplane model [13], while the coarse aggregate (granite stone) is assumed as linear elastic. For illustration, the typical set of mechanical properties of mortar and concrete is summarized in Tab. 1. For the required macroscopic concrete properties, the parameters of the microplane model [13] for mortar were calibrated by trial and error.

In the transient 3D FE analysis, the total strain tensor (ε_{tot}) is decomposed into elastic (ε_{el}) and damage (ε_{dam}) strains (microplane), and the time-dependent non-elastic strains (basic creep (ε_{bcr}), shrinkage (ε_{shr}) and thermal strains (ε_{th})):

$$\varepsilon_{tot} = \varepsilon_{el} + \varepsilon_{dam} + \varepsilon_{bcr} + \varepsilon_{shr} + \varepsilon_{th} \quad (2)$$

Basic creep of the mortar is simulated using generalized Maxwell chain model (rate-type creep law with eight age-dependent units [14]), which is coupled in the series with the microplane model (see Fig. 2). The parameters of the model (relaxation spectra [15]) are chosen such that that the creep factor for loading age $t_0 = 28$ days is approximately four. The creep curves which correspond to the loading age $t_0 =$ 7, 28, 90 and 365 days are shown in Fig. 2c.

Table 1: The resulting mechanical properties of mortar (microplane model) and concrete (meso-scale FE model)

Mechanical properties	Concrete	Meso-model	
		Aggregate	Mortar
Initial Young´s modulus, E [GPa]	39.0	70.0	35.0
Poisson' ratio, v	0.18	0.18	0.18
Compressive strength, f_c [MPa]	54.0	/	50.0
Tensile strength, f_t [MPa]	3.30	/	4.0
Fracture energy, G_F [J/m^2]	65.0	/	45.0

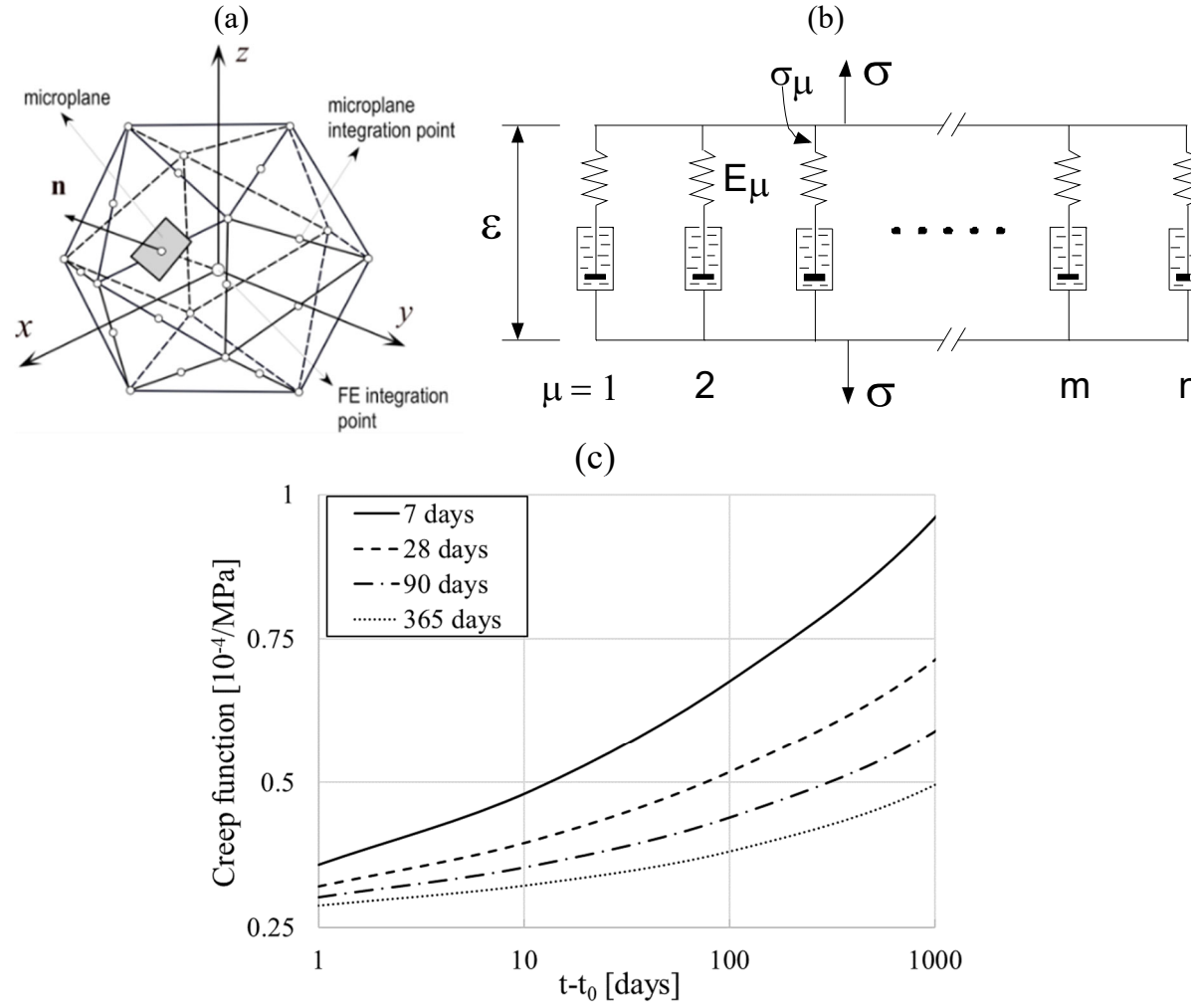

Fig. 2: (a) Microplane model for mortar (21 integration points) [13], (b) generalized Maxwell chain model based on the rate type creep law [15], and (c) typical basic creep functions (compliance) for the loading age of $t_0 = 7$, *28, 90 and 365 days*

In the recent numerical study [16] a simplified approach was used to calculate shrinkage of mortar matrix, i.e., it was calculated by means of an algebraic formula [3], which represents the mean shrinkage of the cross section of the test specimen:

$$\varepsilon_{shr}(t,t_0) = \varepsilon_{shr\infty} k_h S(t) \tag{3a}$$

$$S(t) = \left(\frac{t}{\tau_{shr} + t}\right)^{1/2} \tag{3b}$$

$$k_h = 1 - 0.95h - 0.25h^{200} \tag{3c}$$

where t_0 is the curing time (in days), t is duration of drying (in days), $\varepsilon_{shr\infty}$ is the ultimate shrinkage, k_h is the humidity coefficient, h is the relative humidity, $S(t)$ is a function of t giving the shape of the shrinkage curve and τ_{sh} is the shrinkage square half time. The main assumption of this simplified approach (Eq. 3) is that the relative humidity (h) inside the specimen is constant and equal to the environmental relative humidity (RH). However, in the present study, a more realistic approach is adopted to calculate shrinkage of mortar, by using the 3D chemo-hygro-thermo-mechanical (CHTM) model recently developed for concrete at the University of Stuttgart [17, 18].

For the constant temperature and non-saturated conditions, the moisture mass conservation together with the corresponding constitutive law for moisture transport, can be expressed as [18]:

$$\rho_w \frac{\partial \theta_w(h)}{\partial t} = \rho_w \frac{\partial \theta_w(h)}{\partial h}\frac{\partial h}{\partial t} = \nabla(\delta_v(h) p_{v,sat} \nabla h)$$

$$\delta_v(h) = \alpha_0 f_1(h); \quad f_1(h) = \alpha + \frac{1-\alpha}{1 + \left(\frac{1-h}{1-h_c}\right)^4} \tag{4}$$

where $p_{v,sat}$ is the saturated water pressure [Pa], $h = \rho_v / p_{v,sat}$ is the relative pore pressure, ρ_w is the density of water [kg of water/m^3 of water], θ_w is the volume fraction of pore water [m^3 of water/m^3 of concrete], δ_v is the water vapor permeability [s], t is the time [s], α_0 is the reference permeability at 25 °C, α = 0.05 and h_c = 0.75 at 25 °C. In the incremental transient FE analysis, the main adsorption and desorption curves of concrete are given as input [18]. The sorption isotherms,

experimentally obtained for normal strength concrete with w/c = 0.48 and employed in the present study, are shown in Fig. 3.

In the present numerical study, for the given environmental loading conditions, the distribution of relative humidity h in concrete was computed by solving the weak form of Eq. 4 using 3D finite elements (implicit direct integration) with the corresponding environmental (boundary) conditions. The moisture content θ_w was then calculated by employing the sorption curve for concrete shown in Fig. 3 [18]. To predict shrinkage strain, the relative humidity h was used to calculate the humidity coefficient k_h (Eq. 3c) for each integration point of the finite elements.

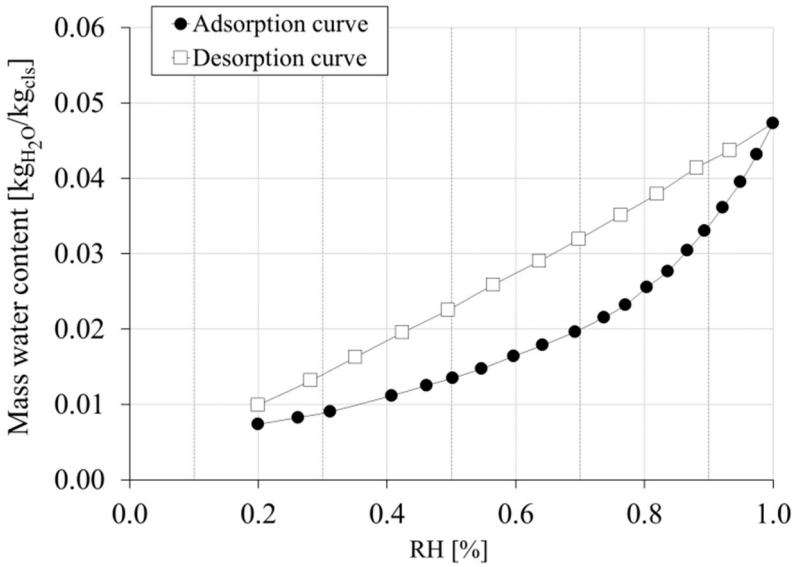

Fig. 3: Adsorption and desorption curves taken from the experiments of Hansen et al. [17]

In the analysis the environmental boundary conditions are defined on the nodes of the exposed specimen surfaces (moisture flux) as:

$$n \cdot j_{w,vol} = \beta_{hum}(h_s - RH) \tag{5}$$

where n is the normal to the exposed surface, β_{hum} is the surface humidity transfer coefficient [m/s], which controls the moisture uptake and consequently the speed of the drying process, h_s is the relative humidity at the surface of the specimen and RH is the environmental relative humidity. If the velocity of the air is relatively high, it can be assumed that $h_s = RH$.

3. CALIBRATION OF THE FE MODEL

In the framework of the model calibration, the mechanical and non-mechanical properties of the meso-scale model were properly set to realistically reproduce the short- and long-term deformations and the failure of concrete. The mechanical properties of the meso-scale model were calibrated such that the numerical data fit the corresponding test data, as mentioned above. The model parameters for the calculation of distribution of *RH* (Eq. 4) are based on the data from [8]. However, the parameters relevant for the shrinkage strains (Eqs. 3,4) were chosen to approximately fit the experimental tests performed in [8] and [19].

3.1 Distribution of relative humidity

In the experimental studies reported in [12] and [11], creep and shrinkage strains were measured for concrete age of 14 days. Moreover, the distribution of moisture over the cross-section was not measured nor calculated in [11]. Therefore, in spite to the fact that the specimen geometry from [8] was not the same as in the present simulations, it was decided to calibrate the model based on the results presented in [8]. The experimental tests [8] started at the concrete age of 28 days with the consequence that the contribution of autogenous shrinkage was relatively small.

In the experimental program [8], several prisms (100 x 100 x 450 mm) were tested for drying shrinkage over 331 days and loaded in concentric/eccentric compression to evaluate the creep behavior. The mean concrete cube compressive strength was f_{cc} = 54.4 MPa (f_c = 45 MPa) and $w/c = 0.4$. After curing period of 28 days all the specimens were kept at the temperature of $T = 20\pm2$ °C and $RH = 70\%\pm10\%$. The axial strains were measured with two wire strain gauges installed on the two opposite faces of each specimen ($\cong 150$ mm length).

The numerical curves from [8] are shown in Fig. 4 in terms of the distribution of relative humidity together with the results obtained with the here employed HM model. The parameters used for the calculation of relative humidity (Eq. 4) are summarized in Table 2.

Table 2: The model parameters used in the calculation of the relative humidity distribution

Sorption isotherms ($w/c = 0.48$)	Fig. 3
Reference water vapor permeability α_0 [s]	3 x 10^{-12}
Surface humidity transfer coefficient β_{hum} [m/s]	0.35 x 10^{-5}
Initial relative humidity [%]	98.5
Boundary relative humidity [%]	70

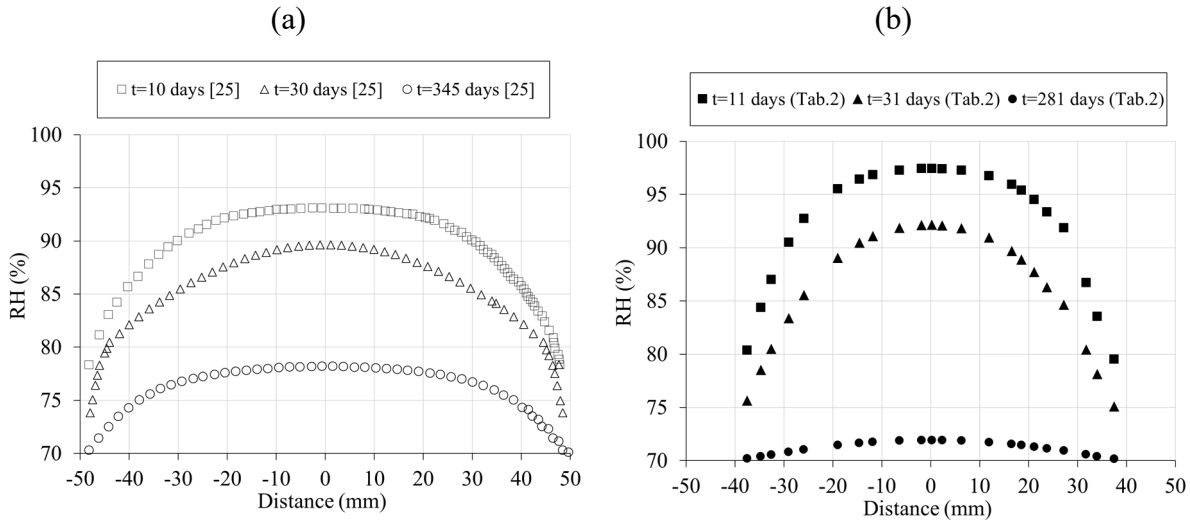

Fig. 4: Distribution of RH across the section: (a) from [8] and (b) calculated using parameters from Tab. 2

Here is made the comparison between the prism with 100 mm section size and the cylindrical specimen with diameter of 76 mm. Fig. 4 shows the distributions of *RH* over the cross-section. They are similar for both geometries and it can be seen that the distribution over the smaller circular section after 281 days of drying is principally almost the same as it is over the slightly bigger square section after 345 days. The time evolution of moisture distribution is also shown in Fig. 5. It can be seen that after 281 days the distribution of *RH* over the cross-section becomes almost uniform.

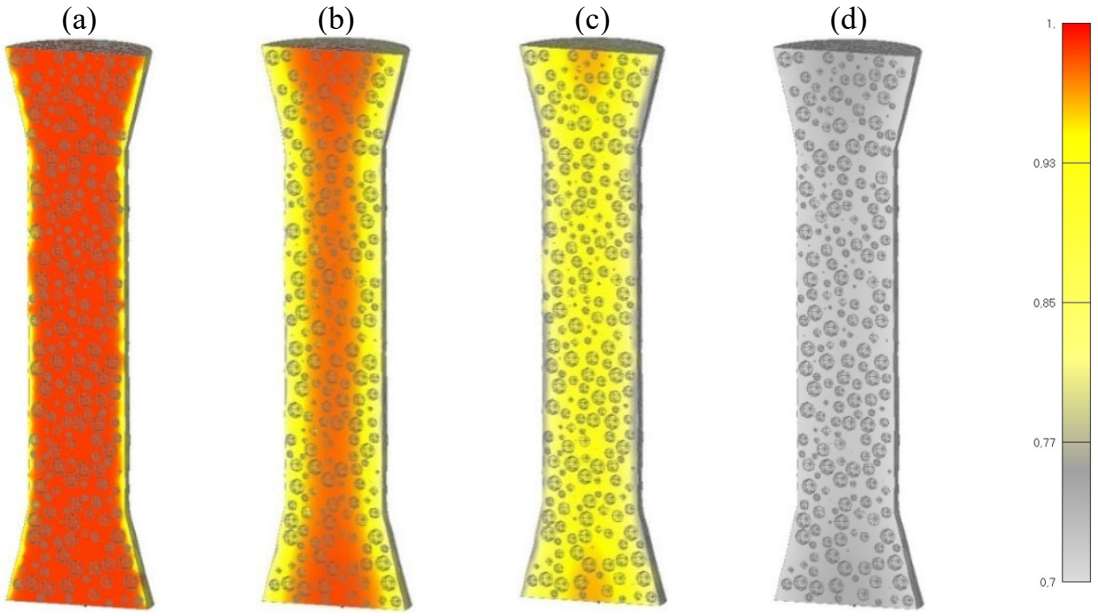

Fig. 5: Distribution of RH across the section: (a) t = 1 day, (b) t = 11 days, (c) t =31 days, (d) t = 281days

3.2 Drying shrinkage of concrete

The shrinkage strain data reported in [8] and [19] were used to calibrate and verify the model. As mentioned above, the specimen was kept at the temperature of 20±2 °C and *RH* = 70%±10% with *w*/*c* = 0.4.

Considering the available data in the literature [8, 19], it was decided to set the initial condition for *RH* to 98.6% and the specimen was dried at 70% and 65% *RH*, the same as in the experiments. The calibrated shrinkage strain curve is shown in Fig. 6a, while the comparison between numerical and experimental results [8, 19] is shown in Fig. 6b.

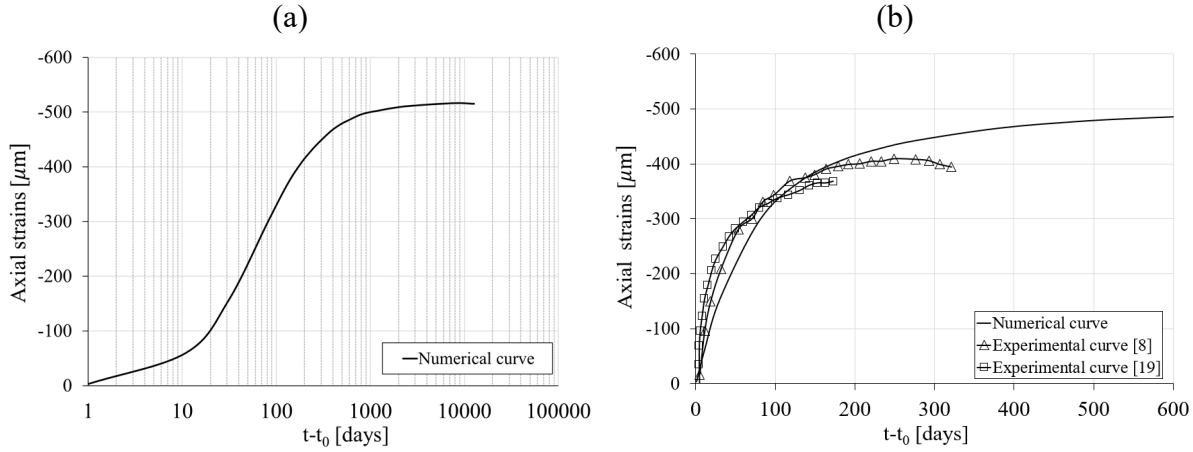

Fig. 6: (a) Shrinkage strain curve (Eq. 3) after 12681 days of drying and (b) shrinkage strain calibration of the numerical model

4. VERIFICATION OF THE FE MESO-SCALE MODEL

4.1 Short-term load

To verify the macroscopic mechanical properties of the meso-scale FE model, the bobbin-shaped specimen was subjected to the uniaxial compressive and tensile load. Fig. 7 depicts the acquired results in terms of axial stress-strain curve and concrete failure mode for uniaxial compression. As can be seen, the meso-scale model is able to realistically represent the typical compressive stress-strain curve of high strength concrete (f_c =54 MPa, ε_c = 0.002, E_c=39 GPa, see Tab. 1) for pre- and post-peak regions (Fig. 7a). The failure mechanism is shown in Fig. 7b in terms of maximum principal strains. The red color indicates the zones with the crack width of 0.10 mm or larger.

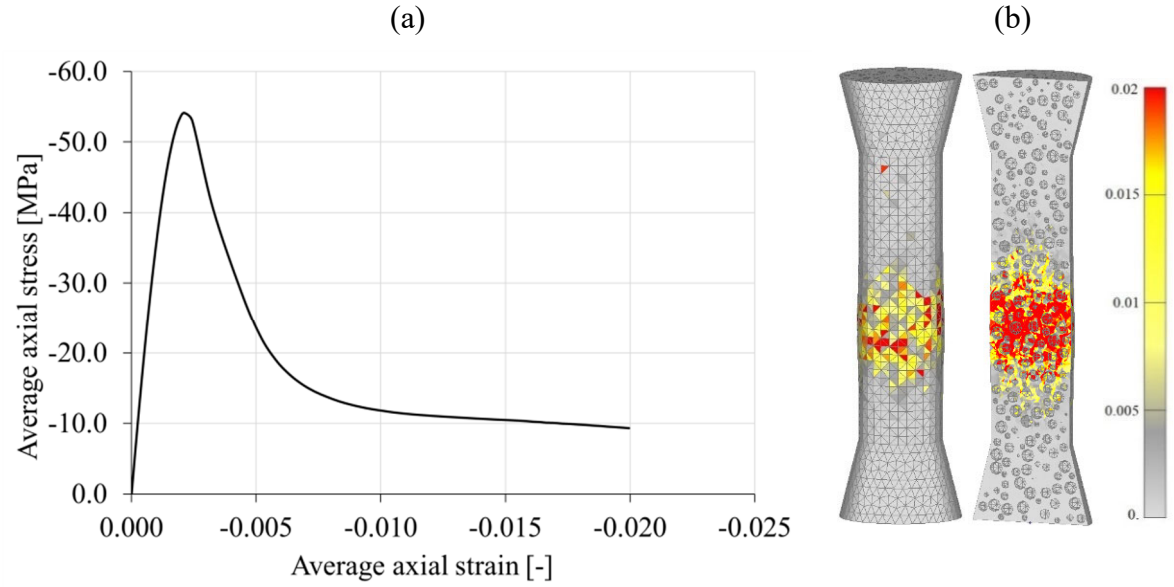

Fig. 7: Uniaxial compression: (a) stress-strain curve and (b) failure mode

The same is shown for uniaxial tension in Fig. 8. The tensile strength of 3.30 MPa is reached and the failure mode corresponds to the localization of a single horizontal crack. Note that the analysis is performed by the displacement control of the specimen top surface.

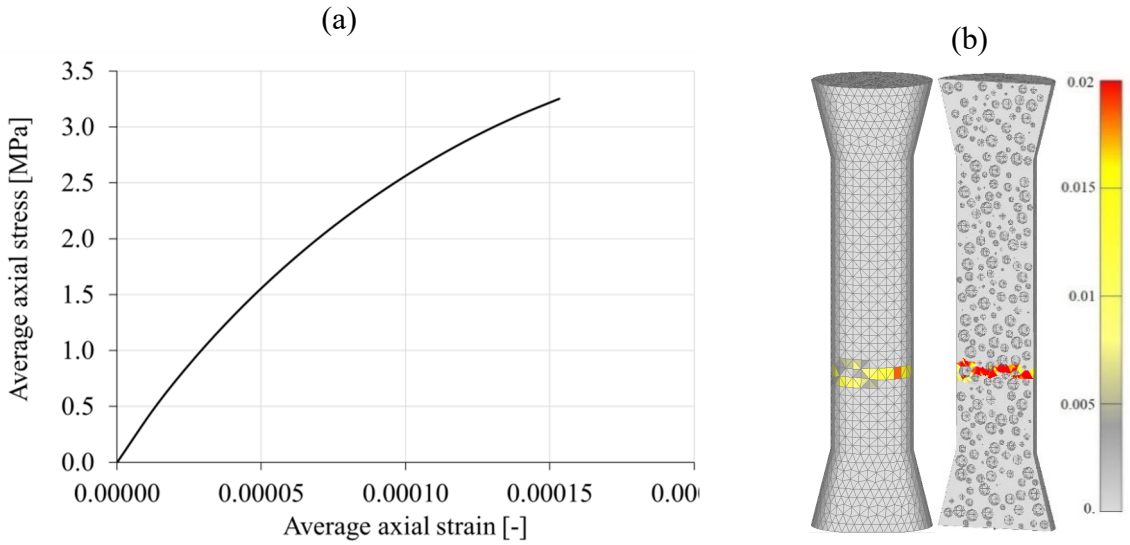

Fig. 8: Uniaxial tension: (a) stress-strain curve and (b) failure mode

4.2 Time-dependent load: creep and shrinkage

To verify the time-dependent response of the model, the numerical results for compressive and tensile time deformations are compared with the experimental results reported in [12, 8]. The experimentally measured drying creep for the load levels of 22% and 55% of the concrete uniaxial compressive strength [8], and for the environmental conditions the same as mentioned above, are shown in Fig. 9 and compared with the model prediction.

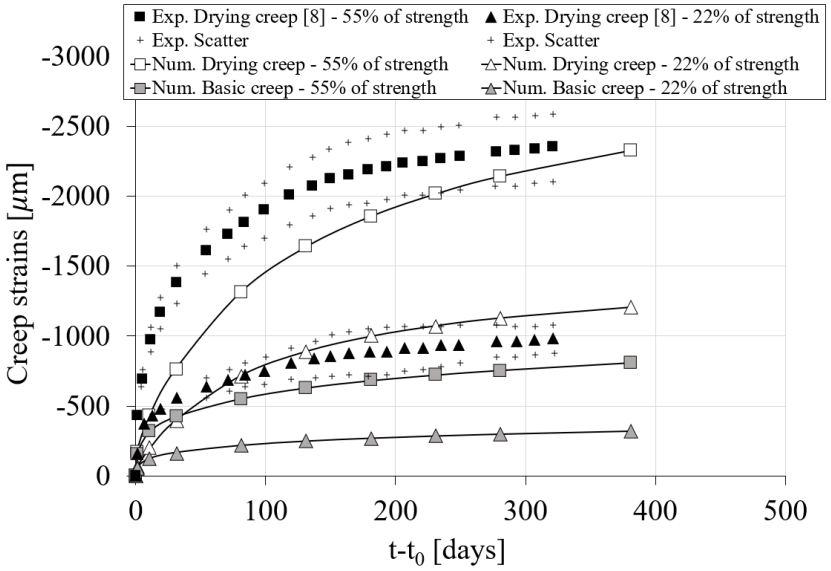

Fig. 9: Comparison between the experimentally measured [8] and computed drying creep for uniaxial compression

According to Eurocode 2, the uniaxial compressive strength of 45 MPa was assumed ($f_c = 0.83 f_{cc}$), i.e., the above-mentioned load levels correspond to 22% and 55% of the uniaxial compressive strength, respectively.

The additional verification for the time-dependent response is carried out for the experimental tests performed by Brooks [12], started in 1972 and running almost last 30 years. The environmental conditions were slightly different compared to the above discussed experiments. The specimens were exposed to 60% of *RH* after 14 days of curing. Moreover, the mechanical properties of the meso-scale FE model were recalibrated based on the uniaxial compressive and tensile strengths of f_c =35 MPa and f_t =1.50 MPa, respectively [12].

The comparison between experimental data and numerical prediction for drying shrinkage is shown in Fig. 10.

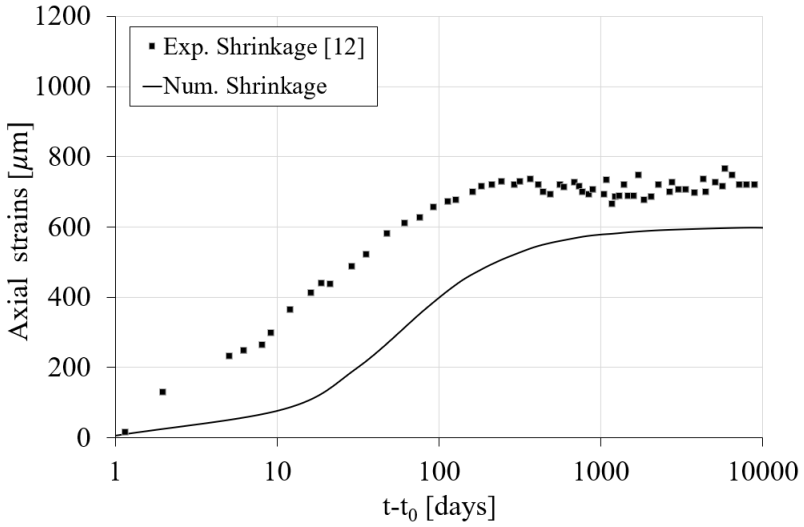

Fig. 10: Comparison between experimental tests [12] and model prediction for drying shrinkage

The basic creep curve and the drying creep curve, which results from the interaction between the applied mechanical load, drying shrinkage and basic creep, are shown in Fig. 11. As can be seen, the basic creep curve (Fig. 11a) shows almost perfect agreement with the measured data. The meso-scale FE model can also well predict drying creep of concrete (Fig. 11b), which is after 27 years approximately doubled compared to the basic creep.

(a)

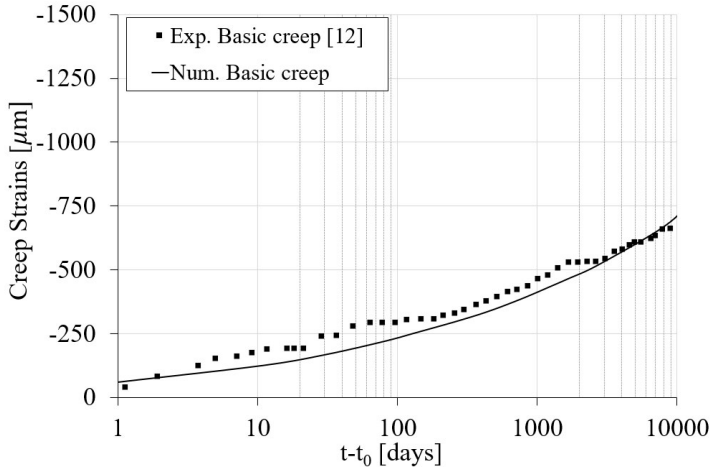

(b)

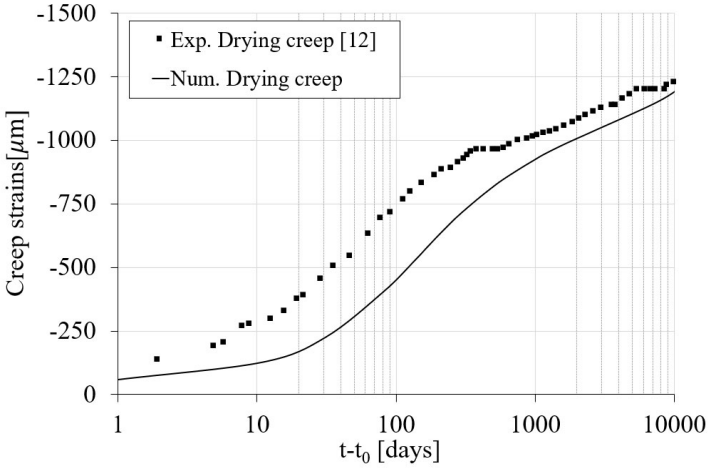

Fig. 11: Comparison between experimental tests [12] and model prediction for: (a) basic creep ($\phi_{lin} = 4$) and (b) drying creep

The verification of the model for basic creep (100% *RH* with the creep factor $\phi_{lin} = 4$) in tension is shown in Fig. 12. The experimental basic creep test from [19] is compared with the model prediction for the stress level of 60 % of uniaxial tensile strength.

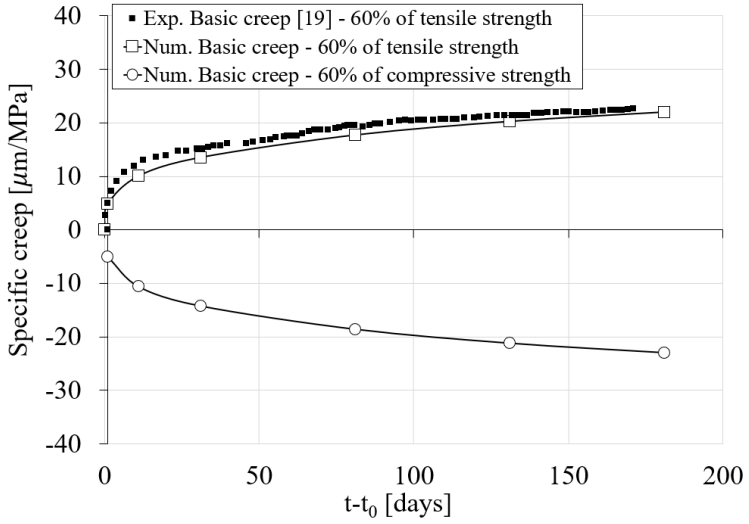

Fig. 12: Comparison between experimentally measured [19] and computed basic creep for uniaxial tension

5. PARAMETRIC STUDY

The parametric 3D FE study at the meso-scale is performed to investigate the influence of the load-induced damage on the time deformation of concrete, i.e. to investigate interaction between non-elastic time deformations of mortar (cement paste) and mechanically induced damage of mortar. The analysis is performed for different mechanical load levels in tension and compression, shrinkage, basic creep and their combination. The mechanical properties of concrete are the same as specified in Tab. 1. In all cases strains are measured from the mid-height of the FE model over the length of 150 mm.

5.1 Shrinkage

The predicted shrinkage curve of concrete without load is already shown in Fig. 6a. It is worth noticing that the final shrinkage of concrete (0.0005) is relatively low with respect to the final value assumed for the mortar (0.0065). This result is justified by the presence of the coarse aggregate, which restraints the specimen volume change.

The results of the shrinkage analysis for different compressive load levels are shown in Fig. 13. It can be observed that as the applied load increases, the non-elastic concrete strains increase significantly, implying that there is a strong interaction between mortar shrinkage and the load-induced damage.

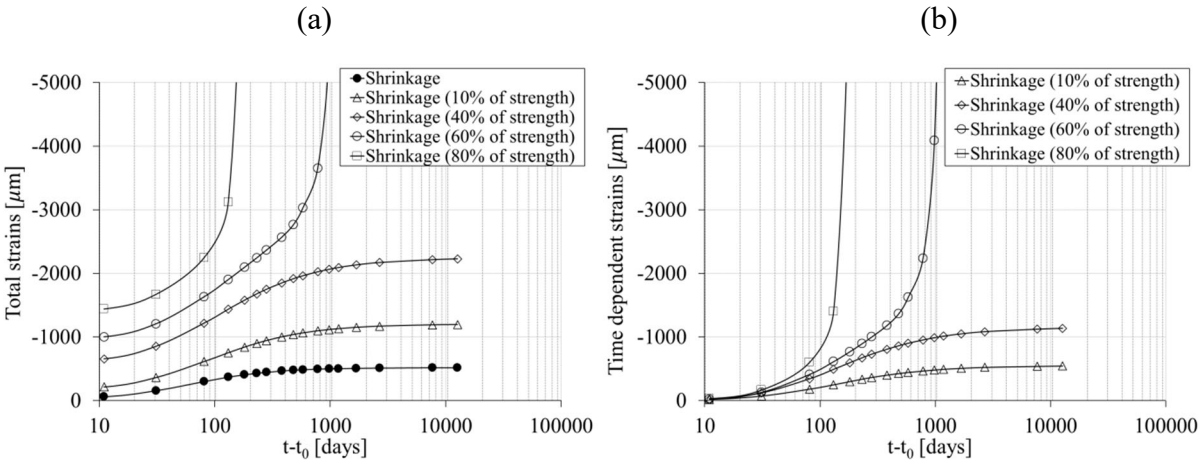

Fig. 13: Average axial total strains (a) and the time-dependent strains (b) of concrete for shrinkage of mortar and mechanical strain

5.2 Basic creep

Fig. 14 shows the average axial strain versus duration of loading for uniaxial compression. It can be observed that when the applied uniaxial compressive stress is increased, the non-elastic (creep) strains increase as well.

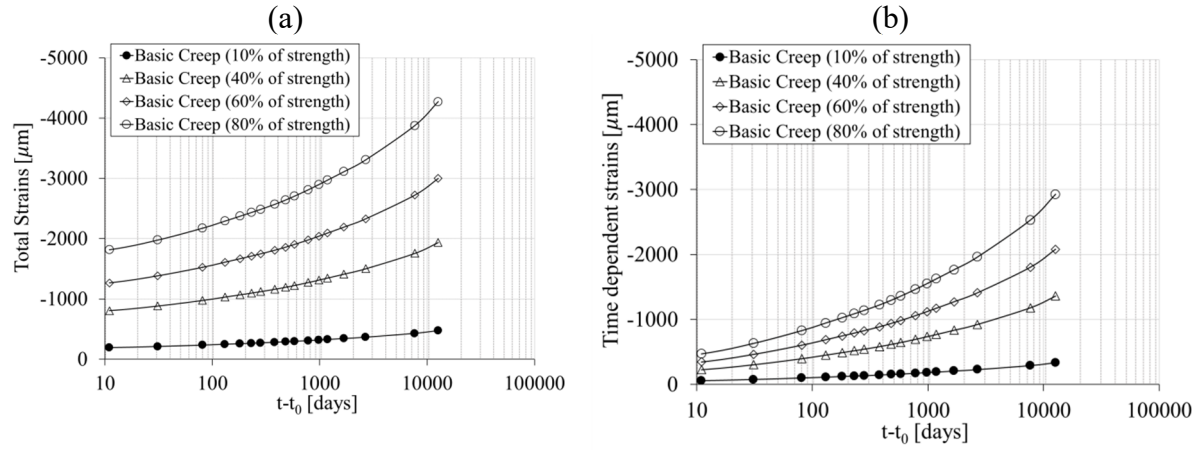

Fig. 14: Average axial total strains (a) and time-dependent strains (b) of concrete for basic creep of mortar and mechanical stress

5.3 Combination of basic creep and shrinkage (drying creep)

To investigate the interaction between load-induced damage, basic creep and shrinkage of mortar, the combined effect of basic creep and shrinkage of mortar was numerically simulated for tensile and compressive load. In Fig. 15 the total axial strains and the corresponding specific creep are plotted versus duration of loading.

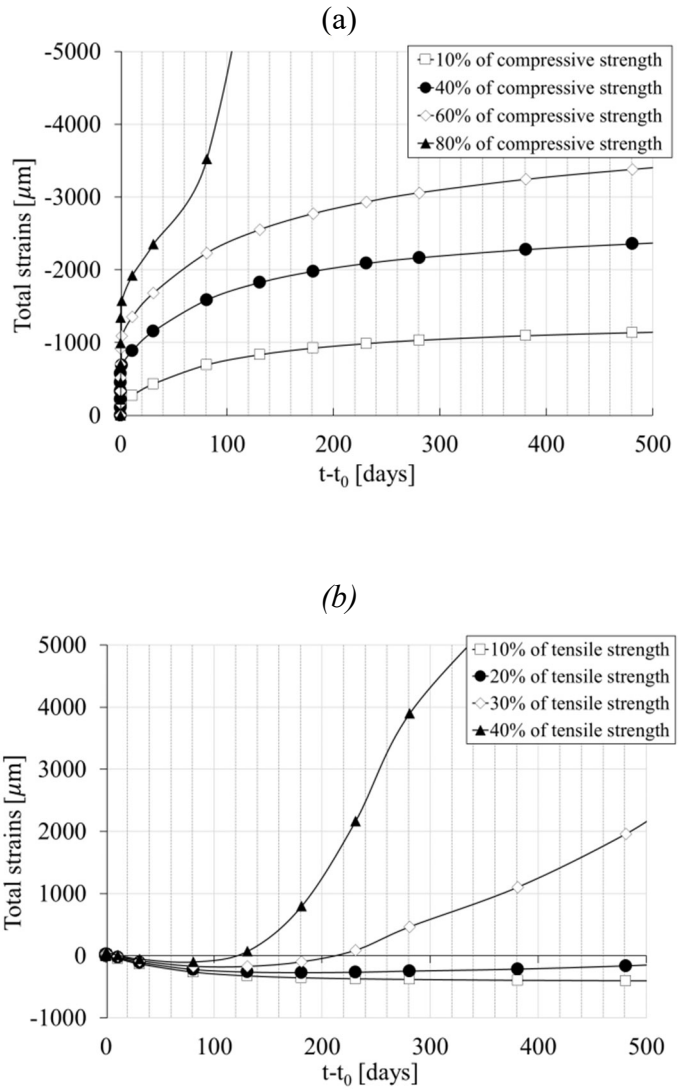

Fig. 15: Axial average total creep of concrete for drying creep: (a) compression and (b) tension

6. CONCLUSIONS

The main aim of the present study was to numerically investigate the interaction between the load-induced damage of concrete (mortar), non-elastic time deformations and heterogeneity of concrete. Based on the obtained results the following can be concluded: (i) The employed meso-scale FE model is able to realistically reproduce the experimental tests for shrinkage, basic creep and drying creep; (ii) It is shown that there is a strong interaction between drying shrinkage and load-induced damage of mortar. (iii) For tensile load the interaction between drying shrinkage and load-induced damage is even stronger and leads to the sustained tensile strength of only $0.40f_t$; (iv) The results show that there is no strong interaction between the load-induced damage and basic creep. To confirm the numerical prediction, the experimental tests are currently running at MPA, University

of Stuttgart; (v) Basic creep has positive effect on drying creep of concrete in compression because it partly compensates the load-induced damage due to drying shrinkage of cement paste; (vi) The numerical simulations indicate that the heterogeneity of concrete has significant contribution to drying creep. (vii) Considering that only a combination of incomplete experimental data sets was used for calibration and validation of the model, further numerical and experimental studies are needed to better understand and clarify the role of interaction between non-elastic time deformations of mortar, damage and heterogeneity of concrete.

REFERENCES

[1] FAHMI, H.M., POLIVKA, M., BRESLER, B.: *Effect of sustained and cyclic elevated temperature on creep and concrete*, Cement and Concrete Res., 2 (1972), 591-606

[2] ROSS, A.D.: *Creep of concrete under variable stress*, American Concrete Institute Journal, 1972, 54: 739-758

[3] BAŽANT, Z.P. OSMAN, E., THONGUTHAI, W.: *Practical formulation of shrinkage & creep of concrete*, Matériaux et Constructions, 1976, 9 (54): 395-406

[4] BAŽANT, Z.P., WENDNER, R.: *Material model & structural analysis model B4 for creep, drying shrinkage & autogenous shrinkage of normal & high-strength concretes with multi-decade applicability*. Mater. Struct., 2015, 48(4): 753-770

[5] TORRENTI, J.M., ROY, R.L.: *Analysis of some basic creep tests on concrete and their implications for modeling.* Struct. Concr., 2018, 19(2), 483-488

[6] GASCH, T., MALM, R., ANSELL, A.: *A CHTM model for concrete subjected to variable environmental conditions*, Int. Journal of Solids and structures, 2016

[7] BAŽANT, Z., NAIJAR, L.J.: *Nonlinear water diffusion in nonsaturated concrete*, Matériaux Et Construction, 1972, 5(1); 3-20.

[8] HUANG, H., GARCIA, R., HUANG, S.S., GUADAGNINI, M., PILAKOUTAS, K.: *A practical creep model for concrete elements under eccentric compression*, Materials and Structures, 2019, 52:119, https://doi.org/10.1617/s11527-019-1432-z

[9] MAZARS, J., PIJAUDIER-CABOT, G.: *Continuum damage theory-application to concrete*, J. Eng. Mech., 1989, 115(2): 345-365

[10] YU, P., DUAN, Y.H., FAN, Q.X., TANG, S.W.: *Improved MPS model for concrete creep under variable humidity & temperature*, Const. & Building Mat. 2020

[11] KRISTIAWAN, S.A.: *Strength, Shrinkage and Creep of Concrete in Tension and Compression*, Civil Engineering Dimension, 2006, 8: 73–80

[12] BROOKS, J.J.: *30-year creep and shrinkage of concrete*, Mag. Concr. Res., 2005, 57(9), 545-556

[13] OŽBOLT, J., LI, Y., KOŽAR, I.: *Microplane model for concrete with relaxed kinematic constraint*, Int. Journal of Solids and Structures 38: 2683-2711, 2001

[14] TAMTSIA, B.T., BEAUDOIN, J.J.: *Basic creep of hardened cement paste A re-examination of the role of water*, Cement and Concrete Research, 2000

[15] BAŽANT, Z., WU, S.T.: *Rate-type creep law of aging concrete based on Maxwell chain*, Matériaux et Constructions, 1974, 7 (37): 45-60

[16] OŽBOLT, J., GAMBARELLI, S.: *Interaction between damage and time-dependent deformation of mortar in concrete: 3D FE study at meso-scale*, 7th Int. Conference on Euro Asia Civil Eng. Forum, IOP Conf. Series: Materials Science and Engineering 615, 2019, 012013 doi:10.1088/1757-899X/615/1/012013

[17] OŽBOLT, J., BALABANIĆ, G., KUŠTER, M.: *3D numerical modelling of steel corrosion in concrete structures*, 2011, Corros. Sci. 53, 4166–4177

[18] OŽBOLT, J., ORSANIĆ, F., BALABANIĆ, G.: *Modeling influence of hysteretic moisture behavior on distribution of chlorides in concrete*, Cement and Concrete Composites, 2016, 67: 73-84

[19] ASSMANN, A., REINHARDT, H.W.: *Tensile creep and shrinkage of SAP modified concrete*, Cement and Concrete Research, 2014, 58: 179–185